Mathematical Models of Adipose Tissue Dynamics

Junghyo Jo, Zeina Shreif, Jonathan R. Gaillard, Matilde Arroyo, Samuel W. Cushman and Vipul Periwal

Abstract Adipose tissue is the main organ for long term storage of energy in the body. Adipose cells store excess energy by enlarging and/or increasing in number, while they provide energy by releasing fat and shrinking as needed. The regulation of energy storage capacity is not a simple problem considering the uncertainty of following food intakes and physical activities. In this Chapter, we introduce the inference of adipose tissue dynamics from adipose cell-size distributions using mathematical modeling and Bayesian inference. We examine recruitment of new adipose cells, growth/shrinkage and death of existing cells under positive/negative energy balance. A comprehensive understanding of adipose tissue dynamics can provide new insights into metabolic disorders such as obesity and diabetes.

1 Adipose Cells

Lipid and glucose are two primary fuels in our body. In particular, lipids are an efficient form for storing energy because of their high calorie density, but they are cytotoxic. Adipose cells store lipids as neutral triglycerides, and protect non-adipose

J. Jo (✉)
Asia Pacific Center for Theoretical Physics, Hogil Kim Memorial Building #542 POSTECH, Pohang, Korea
e-mail: jojunghyo@apctp.org

M. Arroyo · S. W. Cushman
Diabetes, Endocrinology and Obesity Branch, NIDDK, NIH, Bethesda, MD, USA
e-mail: samuel.cushman@nih.gov

Z. Shreif · J. R. Gaillard · V. Periwal
Laboratory of Biological Modeling, NIDDK, NIH, Bethesda, MD, USA
e-mail: zeina.shreif@nih.gov

V. Periwal
e-mail: vipul.periwal@nih.gov

Stud Mechanobiol Tissue Eng Biomater (2015) 16: 11–34
DOI: 10.1007/8415_2013_170

Published Online: 13 December 2013

cells from lipotoxicity [1]. Functional failures of adipose cells result in surplus of circulating lipids, cytotoxic lipid accumulation in liver, muscle, pancreas, kidney, and heart. Finally, the spillover of lipid to non-adipose tissues leads to metabolic disorders such as nonalcoholic fatty liver disease, diabetes, kidney and heart failures. Obesity and lipodystrophy represent two opposite extremes of the pathologies that result from an inability to modulate lipid storage. In addition, aging is a physiological degenerative process that limits efficient lipid storage in adipose tissues [2].

Adipose tissues increase their volume by enlarging cell size (hypertrophy) and/or increasing cell number (hyperplasia). Considering that most eukaryotic animal cells have fixed diameters of a few microns, adipose cells have unique volume flexibility. The largest adipose cells ($\approx$200 μm diameter) are ten times larger than the smallest ones. Note that this diameter difference corresponds to a thousand-fold volume difference. The biochemical processes of lipogenesis and lipolysis underlie the enlargement and shrinkage of adipose cells. Lipogenesis provides free fatty acids, required for triglyceride synthesis, from metabolized products of sugars (e.g., glucose), while lipolysis breaks down triglycerides into free fatty acids. The hormone insulin, a critical hormone for glucose metabolism, is a key regulator of the two processes. Secreted when glucose increases, it suppresses lipolysis and stimulates lipogenesis. Therefore, when glucose availability is high in blood, lipid is not produced, but stored in adipose tissues. On the other hand, under fasting conditions when glucose availability is low, lipid is released and contributes to the generation of glucose via gluconeogenesis. Therefore, insulin plays a crucial role for switching lipogenesis and lipolysis, and thereby insulin resistance affects lipid metabolism.

The plasticity of adipose cell number in adults is not clear, partly because it is technically difficult to accurately measure total adipose cell number. Many reports, including a recent one [3], concluded that the total adipose cell number does not change after early developmental periods. However, adipose cell number can still increase in adults under stimulating conditions such as lipectomy (partial excision of adipose tissues) and high-fat diet [4, 5]. In the diet-induced volume expansion of adipose tissues [5], Faust et al. demonstrated that when adipose cells exceed a certain critical size, they stimulate the recruitment of new cells, suggesting that hypertrophy is a default option for small demands on increasing the lipid storage capacity, while hyperplasia is a backup one for extreme demands as adipose cells cannot grow indefinitely. Here hyperplasia is irreversible, while hypertrophy is reversible. Once hyperplasia occurs, due to obesity, the new adipose cells remain even after losing weight. The irreversibility of hyperplasia may explain the "yoyo" effect of easily regaining lost weight.

Adipose tissue growth via hypertrophy has the advantage of reversibility, but the disadvantage of limited expansion capacity. Considering that lipid uptake/release occurs through the cell surface, larger cells are less efficient at transferring lipids through the cell surface due to their decreased surface-to-volume ratio. In addition, it has been reported that large adipose cells are involved with hypoxia [6], inflammation [7], cell death (necrosis/apoptosis)[8], and physical fragility [9].

Therefore, whenever adipose tissues meet the expansion demands, they have to make a decision whether to enlarge existing resources or to recruit new resources that have flexible expansion potential, but cannot be removed without possibly inflammatory processes such as necrosis and apoptosis once they have appeared. There may not be a universal strategy since different fat depots have different cellularity; epididymal fat depot rely on hypertrophy, while subcutaneous fat depots rely on both hypertrophy and hyperplasia [4]. People in developed countries rarely experience uncertainties in future food intake, but animal models can be used to probe the regulatory response of adipose tissue to ensure energy homeostasis under changes in food availability.

Unfortunately, currently available experimental techniques are not capable of direct measurements of the complicated dynamic processes of adipose tissues. In this Chapter, we introduce a Bayesian method that infers the dynamic processes from changes of static snapshots of adipose cell-size distributions. The mathematical modeling explains detailed physical processes of adipose tissue expansion/shrinkage, and suggests microscopic origins of metabolic disorders in obesity and diabetes.

2 Bimodal Size Distribution

The size of adipose cells is usually observed by microscopes with the histological preparation of adipose tissue sections. This conventional method has the well-known limitations of small sample number and uncertainties in diameter measurements as the locations of the centers of the cut cells relative to the tissue section are unknown. To address the latter issue, isolated suspension of adipose cells has been used for microscopic observations [10]. Another popular and powerful method is the automatic counting and sizing of adipose cells fixed by osmium tetroxide [11]. The Coulter multi-sizer determines sizes of such fixed cells by measuring conductivity changes due to the obstruction produced by cells going through an aperture. This allows fast unbiased measurement of large numbers of fixed adipose cells. The precise histograms of adipose cell sizes measured by the multi-sizer always give bimodal size distributions of adipose cells (Fig. 1), while the conventional microscopic measure frequently produces unimodal size distributions that ignore the left peak of small cells in the bimodal size distribution. The lower peak, measured by the multi-sizer, has been criticized on the grounds that it may have originated from particles broken from fixed adipose cells. However, computerized measurements with higher microscopic resolution have also observed the bimodal size distribution in the isolated suspension of adipose cells [10]. Therefore, the lower peak seems to be real, although the multi-sizer observation may somewhat exaggerate it.

As suggested in McLaughlin et al. [12], the bimodal distribution can be approximately fitted with two exponentials and one Gaussian function. Therefore, it is tempting to interpret the origin of the bimodality as two cell populations of

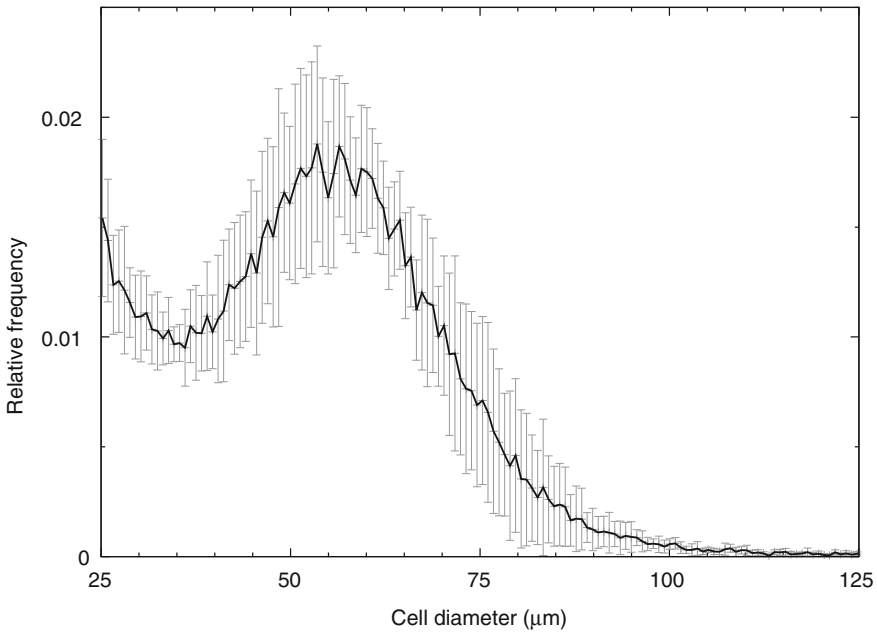

Fig. 1 Bimodal size distribution of adipose cells. Adipose cells from epididymal fat depots in C56BL/6 mice (male and 3 months old) were isolated, and relative frequencies of their diameters were measured by a Coulter multi-sizer. Mean ± SD (n = 6)

preadipocytes and mature adipose cells. The exponential part consisting of small cells may represent new cells recruited from progenitor cells, while the Gaussian part may represent larger mature cells that have grown from the small ones. A hypothetical dynamic model for the bimodal distribution will be discussed later. On the other hand, Soula et al. [13] have recently proposed that the origin of the bimodality is a singularity in the size-dependent growth rate of adipose cells. The cell growth rate results from the balance between lipogenesis and lipolysis, both of which depend on adipose cell size. The size-dependent growth rate has an unstable singular size at the nadir size of the bimodal distribution. Therefore, cells below this critical size shrink to smaller sizes while those above it can grow to larger sizes. Another perspective from the viewpoint of stochastic modeling of adipogenesis in cell culture can be found in [14, 15], taking into account the accumulation and formation of lipid droplets within adipocytes.

3 Bayesian Inference

As discussed above, the adipose tissue dynamics is intricate and requires further investigation. However, current experimental techniques are not capable of monitoring such changes in real time. Nevertheless, precise measurements of

adipose cell-size distributions at discrete time points can be used to theoretically examine the dynamic processes (e.g., cell recruitment, growth/shrinkage, and death) in adipose tissues, because cell-size distributions reflect what adipose cells experience during their life span. We introduce a Bayesian method to deduce longitudinal information from changes of the cross-sectional information of adipose cell-size distributions measured at different times. Bayesian inference has been applied to understand not only the adipose tissue dynamics [16, 17], but also pancreatic islet development [18].

Given the mean and uncertainty of measured frequencies, m_i and δm_i at the ith bin, the maximum entropy principle [19] gives the likelihood of predicted frequencies $n_i(x)$ of a model M associated with a set of parameters x as

$$P(D|x,M) \propto \prod_i \exp\left[-\frac{\left(m_i - n_i(x)\right)^2}{2\delta m_i^2}\right] = \exp[-E(x)], \tag{1}$$

where the mismatch between the measurement and prediction is quantified as a cost,

$$E(x) = \sum_i \frac{\left(m_i - n_i(x)\right)^2}{2\delta m_i^2}. \tag{2}$$

In this chapter, the model M will be a dynamic model that predicts the evolution of adipose cell-size distributions m_i. The set of parameters x represents physical processes such as recruitment, growth, death rates, and their size dependences.

Bayes' rule (or product rule in probability theory) gives the posterior probability distribution of the parameter set x, given data D and model M [20]:

$$P(x|D,M) = P(x|M)\frac{P(D|x,M)}{P(D|M)} = \frac{P(x|M)\exp[-E(x)]}{\int dx\, P(x|M)\exp[-E(x)]}, \tag{3}$$

where $P(x|M)$ is the prior distribution of x, usually set as constant with the assumption of complete ignorance. Using the probability $P(x|D,M)$, it is straightforward to compute the mean and uncertainty of parameter x:

$$\bar{x} = \int dx\, xP(x|D,M), \tag{4}$$

$$\delta x^2 = \int dx\, x^2 P(x|D,M) - \bar{x}^2. \tag{5}$$

Monte Carlo (MC) methods are usually used to compute these, because the update in MC is determined by the probability $P(x|D,M)$.

Generally we can propose several hypothetical models to explain the given data. Bayesian model comparison is particularly appropriate in such a context because Bayes' rule balances model complexity and goodness of fit. An overly

complex model is less likely to give robust predictions, especially since most biological datasets are much smaller than the complexity of the underlying processes would require for a complete fit. Model selection can be done using the Bayes factor comparing two models, M_1 and M_2:

$$\frac{P(D|M_1)}{P(D|M_2)} = \frac{\int dx_1 \; P(D|x_1, M_1)P(x_1|M_1)}{\int dx_2 \; P(D|x_2, M_2)P(x_2|M_2)}. \tag{6}$$

The Bayes factor can be easily computed if we introduce a temperature parameter. We define a partition function in analogy with statistical physics (generating function in probability theory):

$$Z(\beta) = \int dx \; P(x|M) \exp[-\beta E(x)], \tag{7}$$

where β represents the inverse temperature. Small values of β correspond to high temperature, while large β corresponds to low temperature. As in statistical physics, the parameter sets x that contribute significantly to Z at high temperature are determined more by the volume of the parameter space and less by the goodness of fit embodied in E. At low temperature, only configurations that fit the data very well contribute to Z. Using the partition function, we can show that

$$-\frac{\partial}{\partial \beta} \ln Z = \frac{\int dx \; E(x)P(x|M) \exp[-\beta E(x)]}{\int dx \; P(x|M) \exp[-\beta E(x)]} = \bar{E}_\beta, \tag{8}$$

relating the average cost at a given β with the logarithmic derivative of the partition function. Therefore, by integrating this relation the partition function can be obtained by computing the cost at different temperatures:

$$-\ln Z = \int d\beta \bar{E}_\beta. \tag{9}$$

Thus, the model likelihood normalized by a summed probability for all models, $P(D) = \sum_i P(D|M_i)$, corresponds to the partition function for $\beta = 1$:

$$\frac{P(D|M)}{P(D)} = Z(1) = \exp\Big[-\int_0^1 d\beta \bar{E}_\beta\Big]. \tag{10}$$

This is practically very useful when we use MC methods. Such parallel tempering MC methods are powerful tools for exploring the cost (or energy) landscape because high temperature is suited to searching the global landscape, while low temperature is good for searching fine landscape. Therefore, parallel tempering MC methods can take both advantages to find a global minimum. In addition, the parallel tempering MC using multiple temperatures allows to automatically compute the average costs $\bar{E}_\beta$ at different temperatures, and finally the temperature integration in Eq. (10) [21]. In summary, Bayesian inference can estimate likelihood values of parameters of models given data, and quantitatively compare different models.

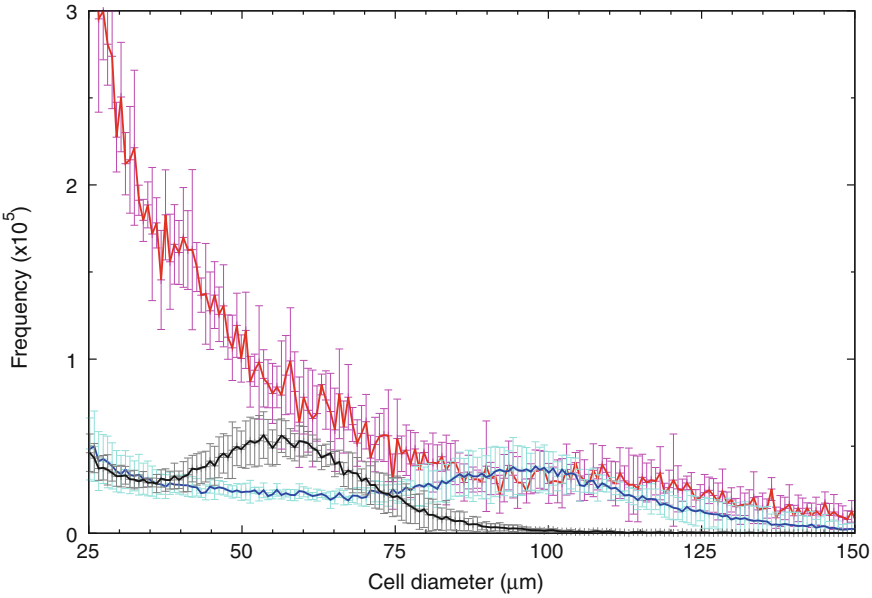

Fig. 2 Evolution of adipose cell-size distribution under positive and negative energy balance. C56BL/6 mich were fed with a high-fat diet for 7 weeks, then with a regular diet for following 12 weeks. Cell-size distributions in epididymal fat depots were measured at initial time (3 months old; *black*), after 7-week high-fat diet (*red*), and after 7-week high-fat diet plus 12-week regular diets (*blue*). Mean ± SD (n = 6). Note that we estimated absolute frequencies of cell sizes from their relative frequencies by using the measured depot mass of epididymal fat

4 Adipose Tissue Dynamics

The Bayesian method can infer adipose tissue dynamics from changes of static snapshots of adipose cell-size distributions under positive and negative energy balance (Fig. 2). Possible physical processes in adipose tissue dynamics are recruitment of new cells, growth, shrinkage, size fluctuation, and death of existing cells. They can be mathematically summarized in a model described by the following partial differential equation:

$$\frac{\partial n}{\partial t} = b\delta(s - s_0) - \frac{\partial}{\partial s}[v(s)n] + D\frac{\partial^2 n}{\partial s^2} - k(s)n. \tag{11}$$

The equation describes the whole life of adipose cells from birth to death. Here, model parameters represent birth rate b at minimal cell size s_0, size-dependent growth/shrinkage rate $v(s)$, size fluctuation rate D, and size-dependent death rate $k(s)$. Note that we replaced the frequencies n_i at discrete ith size bins with a frequency function $n(s)$ for continuous size s as a continuum limit. Hereafter we examine each process inferred from changes of adipose cell-size distribution under positive and negative energy balance.

4.1 Recruitment of New Adipose Cells

An old hypothesis is that the total number of adipose cells does not increase after a critical developmental period. Although this is partly true for some fat depots such as epididymal fat [4], the hypothesis has been revised due to experimental evidence that new adipose cells can be recruited in adults not only under stimulating conditions such as lipectomy [4] and high-fat diet [5], but also under normal conditions [3]. Spalding et al. [3] have reported that human adipose cells turn over with a period of 10 years, although total cell number is fixed. However, the sources of new adipose cells are still controversial. Pre-existing preadipocytes and stem cells in adipose tissues are potential candidates [22], because mature adipose cells are known to be post-mitotic cells incapable of proliferation [23]. Under weight gain conditions, we have confirmed that small adipose cells ($<25\,\mu$m diameter) are recruited based on the evolution of adipose cell-size distribution under high-fat diet [16]. Furthermore, the recruitment rate strongly depends on genetics as well as diet.

4.2 Size-Dependent Growth/Shrinkage

The growth and shrinkage of adipose cells are basically governed by the biochemical processes of lipogenesis and lipolysis, respectively. Therefore, the growth/shrinkage rate depending on adipose cell size s can be described by two terms:

$$v(s) = v_+(s) - v_-(s). \tag{12}$$

As a simple size dependency, we may assume that both lipogenesis and lipolysis in adipose cells are biochemical processes limited by cell-surface area, if adipose cells are sufficiently mature (i.e., larger than a certain critical size). Note that the critical cell size for the two processes may not be the same in general. This assumption suggests a simple size-dependent growth/shrinkage rate of adipose cells:

$$v(s) = \frac{v_+^m}{2}\left[1 + \tanh\left(\frac{s - s_+}{\eta_+}\right)\right] - \frac{v_-^m}{2}\left[1 + \tanh\left(\frac{s - s_-}{\eta_-}\right)\right] \tag{13}$$

where $v_\pm^m$ represents the maximal lipogenesis/lipolysis rate; $s_\pm$ is the critical size for lipogenesis/lipolysis, which gives the half-maximal growth/shrinkage rate; and $\eta_\pm$ gives their steepness [24]. We confirmed that the function $v(s)$ satisfactorily explains the evolution of adipose cell-size distribution under positive and negative energy balance, and inferred corresponding likelihood values of these parameters [17]. For example, the maximal lipogenesis rate v_+^m has a larger value under high-fat diet, compared with the value under regular diet, that allows the accelerated

growth of adipose cells for storing excess lipid. Furthermore, insulin-sensitizing drugs, thiazolidinediones (TZD), increase the growth rate of adipose cells [25].

Under conditions of large energy imbalance, one process among lipogenesis and lipolysis dominates, and the growth/shrinkage rate $v(s)$ is approximated by either $v_+(s)$ or $v_-(s)$. Therefore, the special condition implies that the growth/shrinkage rate becomes dependent on cell-surface area. The surface-limiting growth/shrinkage means that larger adipose cells become less efficient for storing and releasing lipids. This conclusion based on microscopic phenomena could shed light on the metabolic disorders in obesity where a large number of large adipose cells are working inefficiently.

4.3 Size Fluctuations and Lipid Turnover

Lipids in adipose cells are continually removed by lipolysis and are replaced by newly absorbed lipids in a process called lipid turnover [26]. This turnover can contribute to size fluctuations of adipose cells. Under continuous high-fat diet, the bump in the bimodal adipose cell-size distribution becomes flatter (Fig. 2). Based on the fact that stochastic fluctuations are usually involved in the spread of Gaussian distributions, we added a diffusion term simulating the effects of size fluctuation of adipose cells on the distribution of adipose cell sizes in the model. The physical origin of the size fluctuation is the stochastic movement of lipids across the cell membrane. It turns out that size fluctuations do not contribute much to the spreading of the distribution as they are dominated by the growth factor $v(s)$.

However, we found an active potentiating role for size fluctuations for adipose tissue dynamics. The bimodal size distribution can be divided into a lower peak and a Gaussian bump. The critical cell size at the nadir of the bimodal distribution approximately corresponds to the critical cell size for lipogenesis. Therefore, small cells below the critical size are not capable of growing with the growth process $v(s)$. Nevertheless, the size fluctuation of the small cells can sometimes jump them across the critical cell size. In particular, under high-fat diet, the size fluctuations increase in magnitude. The larger stochastic jumps allow the transition of more small cells into mature cells which are capable of growing. These cells progress to larger sizes and add to the Gaussian bump observed in the adipose cell-size distribution [16].

4.4 Cell Death

It has been frequently reported that larger cells are more susceptible to damage by reactive oxygen species (ROS), hypoxia, and inflammation associated with infiltration of the adipose tissue by immune cells such as macrophages [6–8, 27].

In addition, larger cells are likely to be more fragile to physical stress [9]. Therefore, the size-dependent death rate of adipose cells can be modeled as:

$$k(s) = \frac{k_m}{2}\left[1 + \tanh\left(\frac{s - s_k}{\eta_k}\right)\right], \tag{14}$$

where k_m is the maximal death rate; s_k is the characteristic size giving half-maximal death rate; and η_k is the width of the size dependence transition. The death of adipose cells starts to occur when adipose tissues have to meet continuous demand to enlarge under long-term high-fat diet [28]. Surprisingly, adipose tissue mass starts decreasing after a prolonged period of positive energy balance. This is due to the limited ability of some fat depots such as epididymal fat to keep on expanding to accommodate the excessive demand. Eventually, adipose cell death will dominate over cell growth. To describe this phenomenon, we assumed that adipose cell death starts to occur when overall adipose cells expand too much. This condition is mathematically described by a step function:

$$\Theta(\bar{s} - s_c), \tag{15}$$

where $\bar{s} = \int ds\, sn(s) / \int ds\, n(s)$ is the mean size of adipose cells. Therefore, the death process of adipose cells is active, $\Theta(\bar{s} - s_c) = 1$, only if the mean cell size exceeds a certain critical size s_c, otherwise $\Theta(\bar{s} - s_c) = 0$ [17].

In addition to the passive death of enlarged adipose cells, it has been observed that small cells are removed under negative energy balance [17]. Two hypotheses are possible to explain the removal of small cells. Apoptosis is one simple possibility [29]. Note that this is a programmed cell death to actively remove unnecessary capacity for storing lipids, in contrast to the passive cell death (necrosis) of enlarged adipose cells. The other possibility is that the disappearing small adipose cells may just shrink below an observable size limit ($<25\,\mu m$). Based on Bayesian model comparison, the latter model was more likely to explain the evolution of adipose cell-size distribution under negative energy balance [17]. Therefore, the tiny adipose cells shrinking below the observable size window can reappear when the energy balance turns positive.

4.5 Cell Turnover

Spalding et al. [3] have reported that human adipose cells have a life span of about 10 years. The dynamic processes of adipose cells inferred above can describe their entire lifespan. New cells appear, and experience stochastic size fluctuations. Once a cell reaches a lower critical size, it starts to grow in a size-dependent manner. After reaching another upper critical size, it is removed by cell death. This hypothetical model raises an explicit conjecture that larger adipose cells are older. The processes of removal of old large cells and recruitment of new small ones form a cycle. Indeed, the cycle in individual cells has also emerged in the

evolution of adipose cell-size distributions. Oscillation of adipose cell-size distributions has been observed in rats with a period of about 50 days [30]. This dynamic scenario can also explain the bimodal shape of adipose cell-size distributions. The accumulation of small adipose cells below the lower critical size for size-dependent growth could explain the lower peak in the adipose cell-size distribution.

5 Adipose Tissue Development

Adipose tissue dynamics varies depending on many factors including age and genetic makeup. To account for age-dependent variations, we propose adding a time dependent factor to Eq. (11) as follows:

$$\frac{\partial n}{\partial t} = b(t)\delta(s - s_0) - \frac{\partial}{\partial s}[v(s,t)n] + D\frac{\partial^2 n}{\partial s^2} - k(s)n. \tag{16}$$

The controversy of whether adipose tissues can recruit new cells after a certain development stage or not might be due to a decrease in the birth rate after a critical age. We propose that the birth rate increases with age before adulthood but starts decreasing again after reaching a critical age:

$$b(t) = \begin{cases} b_1 + \frac{2(b_{max} - b_1)}{1+\exp(A-t)/\alpha_1} & \text{if } t \le A, \\ b_2 + \frac{2(b_{max} - b_2)}{1+\exp(t-A)/\alpha_2} & \text{if } t > A. \end{cases} \tag{17}$$

where A is the critical age, b_{max} is the maximum birth rate at the critical age A, b_1 is the birth rate at the start, and b_2 is the minimal birth rate reached at older age (Fig. 3).

5.1 Parallel Tempering as a Model Selection Method

Figure 4 shows the change in adipose cell-size distribution over time taken from a Zucker fatty rat under a regular chow diet.

The aim is to find the simplest model that can best fit the experimental data. In the section above we already included age dependency for the birth rate. To do so for $v(s)$ is, however, less intuitive. $v(s)$ has six parameters that can change with age, v_+^m, s_+, η_+, v_-^m, s_-, and η_-. If we use different values for each of the six parameters at each time step, we end up with too many parameters and thus overfitting the data. For example, in the above case, this will lead to 66 additional parameters.

To decide which of the six parameters shows the most relevant variation, we compare six models, in each of which only one of the parameters is time-dependent,

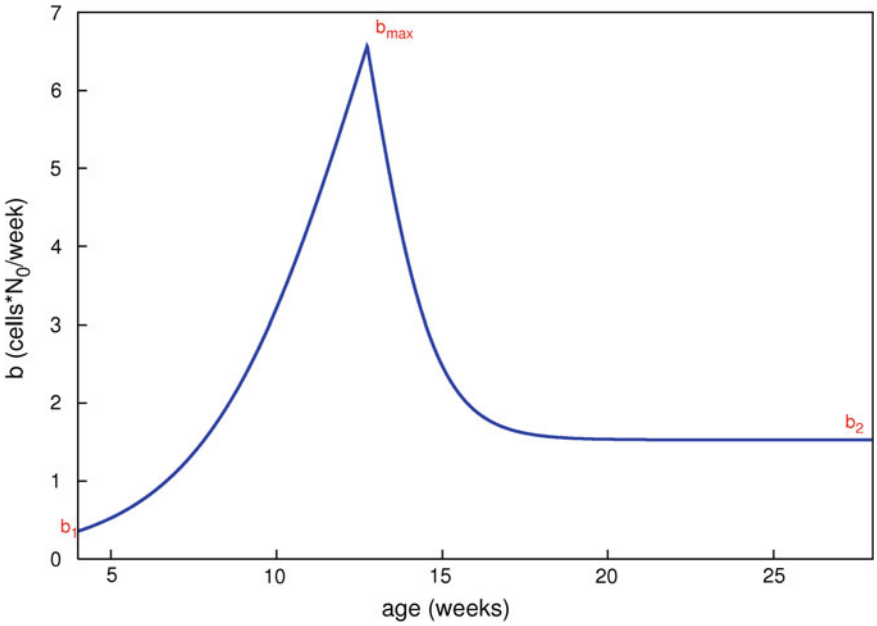

Fig. 3 **Age-dependent birth rate**: Here N_0 is the initial number of cells

and compare them using parallel tempering model comparison. If the aim is to simply find the optimal values then the simulated annealing method [31, 32] would be a better option as it is much less computationally intensive than parallel tempering. Global optimization methods such as simulated annealing provides us with the cost $E_{SA} = E(x)$ of Eq. (2) at the lowest energy point (i.e., at the optimal parameters) but do not take into account the width of the energy landscape. The cost obtained from parallel tempering is $E_{PT} = \int_0^1 d\beta \bar{E}_\beta$. Thus, a lower E_{PT} implies a higher model likelihood as can be seen from Eq. (10).

Tables 1 and 2 show E_{SA} and E_{PT} respectively for the six models fitting 14 different experimental data. The data represent cell-size distribution over time taken from rats fed either a regular chow diet (rats 4 and 5), a high fat diet (rats 6, 7, 8), or under a TZD treatment (rats 12 and 13). At each time point two biopsies are taken, one from the right side and another from the left side. The results show that the most likely model is the one where the steepness of the shrinkage rate η_- vary with time (i.e., η_- takes a different independent value at each time-step).

Another factor that needs to be taken into consideration is a possible correlation between parameters. For example, after examining the correlations between all the parameters, we were able to reduce the model with $\eta_-(t)$ as follows: (1) Parameters b_1 and α_2 of Eq. (17) and the diffusion constant D are kept constant. (2) The cell death is defined as

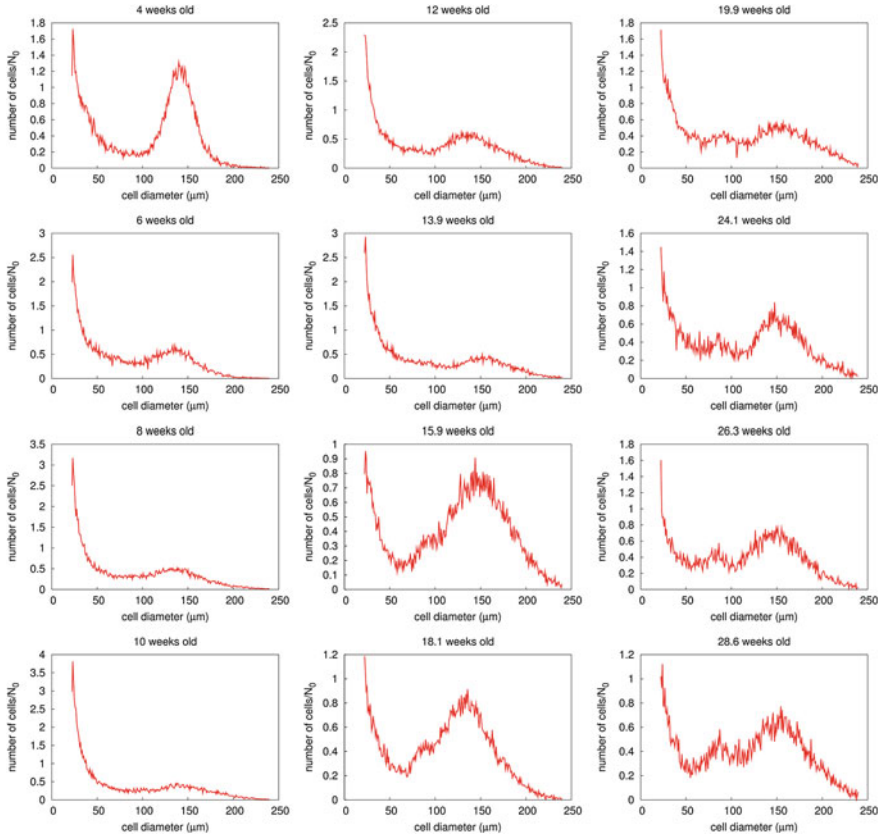

Fig. 4 Adipose cell-size distributions depending on age

$$k(s) = \frac{k_m}{1 + \exp(\alpha_k(S_c - S_v))}\left[1 + \tanh\left(\frac{s - s_k}{\eta_k}\right)\right], \tag{18}$$

where $S_v = \int ds\ s^4(s) / \int ds\ s^3\ n(s)$ is the volume weighted average radius, and k_m, α_k, s_k, and η_k are kept constant. (3) The growth/shrinkage rate is defined as

$$v(s,t) = v_-^m\left[r_v \tanh\left(\frac{s - s_+}{0.5 s_+}\right) - \tanh\left(\frac{s - s_-}{\eta_-}\right)\right], \tag{19}$$

for a constant v_-^m and $r_v = v_+^m / v_-^m$.

Table 3 shows the E_{SA} and E_{PT} results for the reduced (model 2) and non-reduced (model 1) models with $\eta_-(t)$. The non-reduced model, model 1, shows a better fit than the reduced model, model 2, as indicated by the E_{SA} values in Table 3 and Figs. 5 and 6. However, model 2 is more likely as it has much lower E_{PT} values.

Table 1 E_{SA}

Data	$v_+^m(t)$	$v_-^m(t)$	$s_+(t)$	$s_-(t)$	$\eta_+(t)$	$\eta_-(t)$
Rat4 Right	17.11	16.18	16.02	16.94	15.53	15.58
Rat4 Left	15.16	15.02	15.19	16.55	16.75	14.38
Rat5 Right	10.91	12.12	11.50	10.47	12.90	10.67
Rat5 Left	14.63	14.31	12.49	13.93	12.21	12.24
Rat6 Right	8.89	9.10	9.27	9.10	9.73	8.59
Rat6 Left	9.44	10.28	9.88	10.28	10.63	8.31
Rat7 Right	16.73	18.08	17.71	18.21	15.84	15.47
Rat7 Left	11.97	12.00	13.71	12.13	14.87	10.83
Rat8 Right	10.57	9.64	10.03	10.32	10.78	10.15
Rat8 Left	16.28	13.94	13.44	12.91	14.97	13.31
Rat12 Right	7.43	8.51	8.86	8.63	8.54	7.66
Rat12 Left	9.40	9.45	8.12	9.38	8.84	8.62
Rat13 Right	11.61	13.26	13.81	12.93	13.98	12.80
Rat13 Left	15.73	14.98	14.98	13.69	15.22	13.39
Total	175.86	176.86	175.03	175.46	180.8	161.99

Table 2 Model comparison: E_{PT}

Data	$v_+^m(t)$	$v_-^m(t)$	$s_+(t)$	$s_-(t)$	$\eta_+(t)$	$\eta_-(t)$
Rat4 Right	65.75	65.69	63.08	57.09	65.68	57.49
Rat4 Left	63.81	60.73	60.33	56.55	64.61	54.75
Rat5 Right	57.12	55.32	52.80	50.60	61.69	49.83
Rat5 Left	59.02	58.51	55.73	53.51	60.70	53.86
Rat6 Right	50.19	51.57	48.62	44.50	52.12	43.81
Rat6 Left	50.52	50.10	50.35	44.68	56.78	45.08
Rat7 Right	58.78	60.35	57.82	56.70	61.18	52.99
Rat7 Left	55.71	53.28	53.89	47.73	58.97	46.86
Rat8 Right	55.60	58.11	50.91	47.74	57.36	50.13
Rat8 Left	60.96	55.36	54.52	52.68	57.90	53.45
Rat12 Right	44.41	44.31	44.56	39.31	49.49	38.22
Rat12 Left	45.60	45.76	43.55	40.10	48.25	38.71
Rat13 Right	56.36	55.94	55.83	51.25	61.17	50.29
Rat13 Left	60.93	58.40	59.21	55.41	60.57	55.49
Total	784.75	773.44	751.21	697.86	816.47	690.97

6 Adipose Cell Dynamics and Body Composition

In this section we discuss the deduction of physiological processes affecting adipose tissue. The characteristic we consider in this example is the correlation of adipose tissue state with insulin resistance.

Changes in adipose tissue morphology should be reflected in macroscopic body composition. At the macroscopic level, our understanding of the relationship between diet and body composition has improved greatly due to the development

Table 3 Comparing Models 1 and 2

Data	E_{SA}		E_{PT}	
	Model 1	Model 2	Model 1	Model 2
Rat4 Right	15.58	18.42	57.49	43.75
Rat4 Left	14.38	17.95	54.75	42.15
Rat5 Right	10.67	13.06	49.83	36.32
Rat5 Left	12.24	17.64	53.86	39.90
Rat6 Right	8.59	10.43	43.81	31.65
Rat6 Left	8.31	10.33	45.08	30.81
Rat7 Right	15.47	18.48	52.99	43.25
Rat7 Left	10.83	12.69	46.86	35.43
Rat8 Right	10.15	12.28	50.13	33.55
Rat8 Left	13.31	15.66	53.45	38.10
Rat12 Right	7.66	8.21	38.22	26.74
Rat12 Left	8.62	10.23	38.71	27.89
Rat13 Right	12.80	13.92	50.29	35.64
Rat13 Left	13.39	16.26	55.49	39.03
Total	161.99	195.56	690.97	504.21

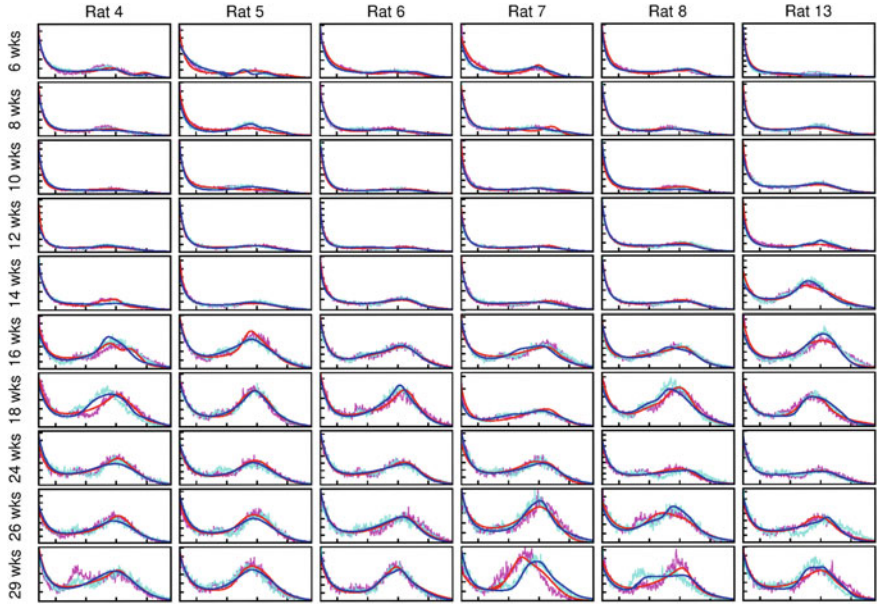

Fig. 5 Adipose cell-size distribution fit with Model 1: Here we show both the adipose cell-size distribution from experimental data (in *pink* for the *right side* and *light blue* for the *left side*) and the corresponding fit using Model 1 (*red* and *dark blue*, respectively)

of predictive mathematical models by Hall and collaborators [33] and others. Apart from transient effects on body composition due to changes in glycogen and water, the fat mass change predicted by these dynamic models of adipose tissue

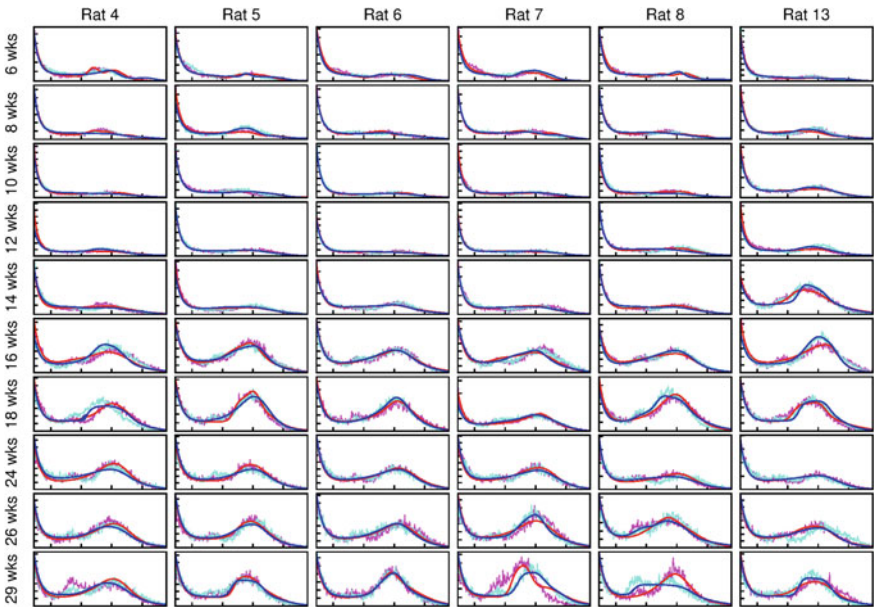

Fig. 6 Adipose cell-size distribution fit with Model 2: Here we show both the adipose cell-size distribution from experimental data (in *pink* for the *right side* and *light blue* for the *left side*) and the corresponding fit using Model 2 (*red* and *dark blue*, respectively)

should agree with the fat mass change predicted by body composition models. This raises a puzzle. Parameters describing adipose cell size distributions are correlated with measures of insulin resistance, so changes in fat mass computed from adipose tissue dynamics will depend on insulin resistance through this correlation with initial adipose cell size distributions [12, 26, 35, 36]. However, the body composition model [33] depends on BMI, gender, age and physical activity level but not on insulin sensitivity. It must follow that parameters determining the dynamics of adipose cell size distributions depend on insulin resistance in a manner that compensates for the insulin resistance dependence of the initial cell-size distributions.

Adipocyte cell-size distribution and physiology data from 28 individuals [12] was separated into six subgroups based on insulin resistance/sensitivity (IR/IS) and/or gender (F/M). Using this data, a body composition model was evolved with isocaloric, weight maintenance diets with different carbohydrate composition 0–100 %, for a period of two weeks. The adipose tissue dynamics model was simplified to exclude effects from increases in cell number. As the time period under consideration is short (two weeks) and the weight change is not dramatic due to an isocaloric diet, this simplification is justified. The majority of the fat that is stored in the fat cells is in larger fat cells as evident in a volume-weighted adipose cell size distribution (Fig. 7). The volume weighted adipose cell size distribution predominantly consists of the cell sizes that are in the Gaussian component of the

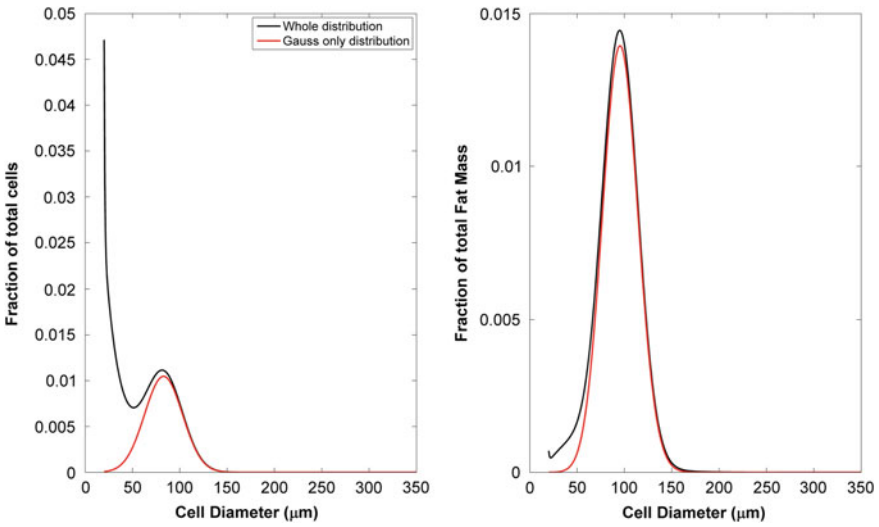

Fig. 7 Gaussian approximation: Most fat mass is in bigger cells

distribution. We therefore used only this component of the adipose cell size distribution to model adipocyte dynamics, using the height, mean, and variance from the patient data. Apart from cell number changing processes, the rest of the model we used is the same as given in the previous sections [16, 17], with a diffusive component with parameter D and a convective component with parameter v_{m0}. The adipose cell size distribution in most individuals is approximated well by a mathematical model composed of two decaying exponentials and one Gaussian distribution [12]. Each distribution was normalized to the total number of cells to account for differences in fat cell number between individuals based on weight.

The body composition models predicted change in fat mass was compared to the prediction from diffusion and convective drift acting on the adipose cell size distribution. A cost function equal to the sum of square differences between the non-transient body composition data from week 1-2 and the adipose tissue models normalized fat mass from week 1-2, computed from the density of fat and the number of cells at each diameter in the distribution. The cost was evaluated for each of the six groups, insulin sensitive (IS), insulin resistant (IR), IS males (ISM), IS females (ISF), IR males (IRM), and IR females (IRF), at different combinations of D and v_{m0} to determine the combination that minimized the cost function. The number of subjects are 15, 13, 4, 11, 4, and 9, for IS, IR, ISM, ISF, IRM, IRF, respectively. Nevertheless, the cost surfaces show that requiring agreement between the predictions of the two models specifies lipid turnover and lipid uptake or release magnitudes.

Cost surfaces show that lipolysis or lipogenesis v_{m0} has a much greater effect on the goodness of fit than the lipid turnover D (Fig. 8). Lipogenesis and lipolysis, represented by convective velocity, have the greater effect since they move the

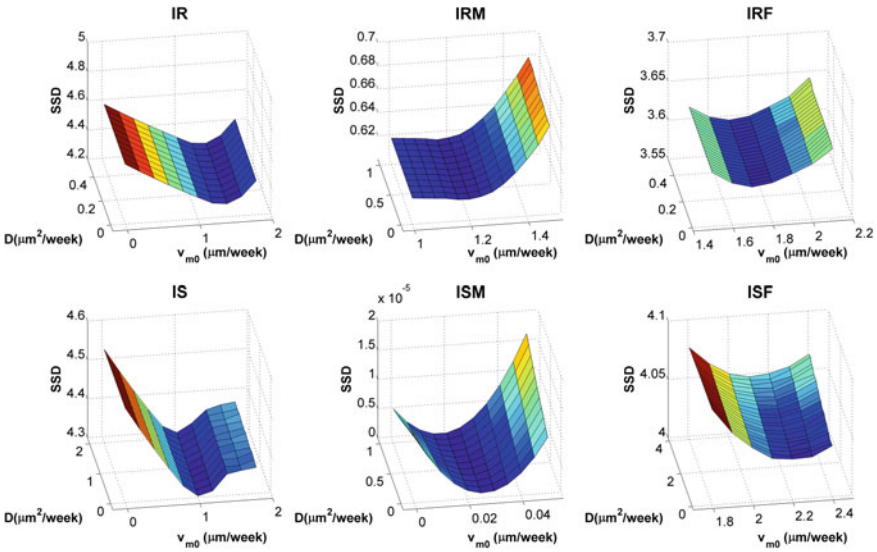

Fig. 8 Lipolysis/lipogenesis have the greater effect on the cost function than lipid turnover: The cost function (sum of square differences (SSD) between adipocyte dynamics and non-transient body composition changes) as a function of lipid turnover (diffusion, D) and lipogenesis/lipolysis (convective velocity, v_{m0}). Groups shown: Insulin Sensitive (IS) and Insulin Resistant (IR), Males (M) and Females (F) at 0 % of total energy from carbohydrates

entire distribution in one direction. As such, it should follow that a larger value for the convective parameter should lead to faster weight gain than a smaller convective velocity. In contrast, lipid turnover is negligible ($D < 10^{-4}$ μm^2/week) in males but not in females. This suggests that lipid is being added to the adipocytes and thus there is very little turnover. This is consistent with the evidence that lipid turnover is higher in women than in men, possibly related to catecholamines [39, 40].

Observing a consistent trend in IRM and ISM in terms of lipid turnover, and lipogenesis and lipolysis under weight gain and weight loss respectively, cost surfaces were computed for both IRM and ISM at a finer resolution using step increases of 10 % in carbohydrate fraction of dietary intake. Weight gain conditions presented differently shaped cost surfaces but weight loss conditions presented almost identical trends (Figs. 9 and 10). At a rate of 10^{-3} μm^2/week, lipid turnover is very small compared to the rate of lipogenesis. This is in contrast to the non-negligible lipid turnover found in the IRF and ISF groups. The minima provide insight into the previously mentioned transient rise and fall in lipid turnover during weight loss. Both IRM and ISM show a peak lipid turnover that then decreases as the carbohydrate percentage in the diet increases. However, the diet at which turnover is maximized is different as IRM peaks at 80 % while ISM peaks at 90 %. Both exhibit a sigmoidal increase in rate of lipolysis from 50 to 100 % of diet from carbohydrates. Under weight gain conditions, ISM exhibits a rapid decrease in the rate of lipogenesis as the carbohydrate percentage increases from 0 to 50 %.

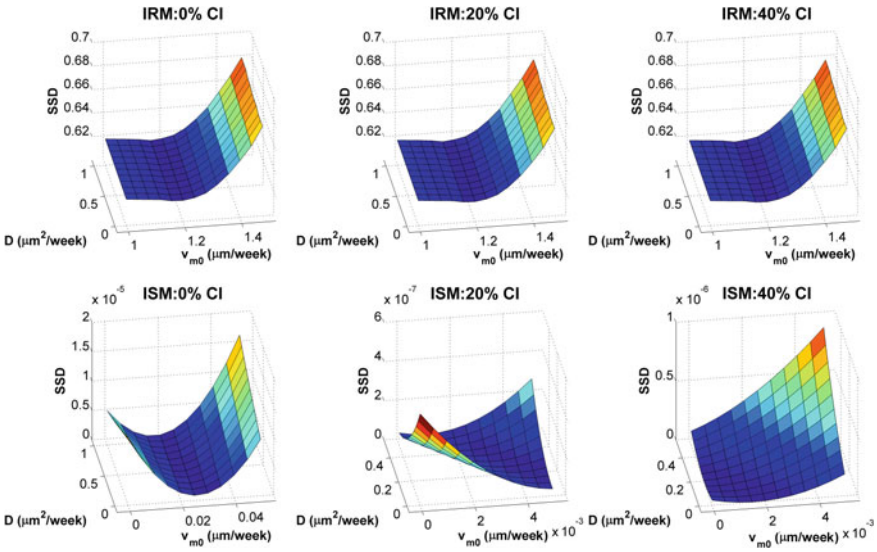

Fig. 9 ISM and IRM demonstrate different cost functions under weight gain yet similar cost functions under weight loss: The cost function as a function of lipid turnover (diffusion, D) and lipogenesis/lipolysis (convective velocity,vm0) for different isocaloric diets of 0, 20, 40 % energy from carbohydrates. Groups shown: insulin resistant males (IRM) and insulin sensitive males (ISM)

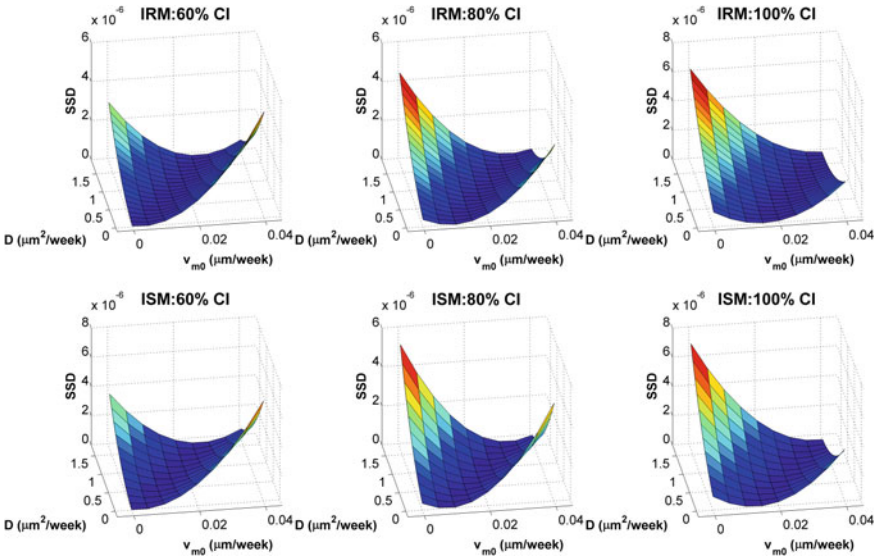

Fig. 10 ISM and IRM cost functions: 60, 80, and 100 % energy from carbohydrates

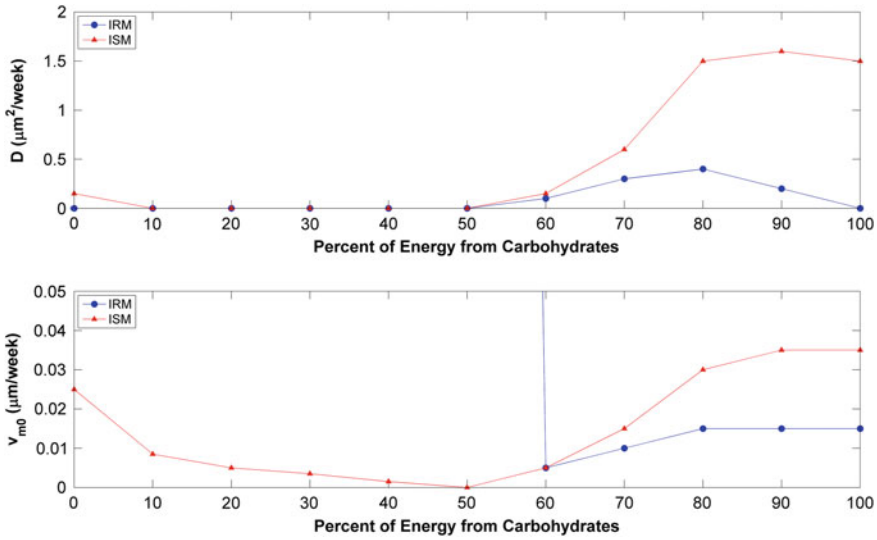

Fig. 11 Comparison of lipid turnover (D) and lipogenesis/lipolysis (v_{m0}) values in IRM and ISM: Comparison of lipid turnover (diffusion, D) and lipogenesis/lipolysis (convective velocity, vm0) values in Insulin Resistant Males (IRM) and Insulin Sensitive Males (ISM) at different isocaloric diets. The lipid turnover for IRM and ISM are both negligible during weight gain and are approximated at zero. Lipogenisis for IRM is 12 m/week (not shown on this scale) for all diets $<50\,\%$ carbohydrate. During weight loss (carbohydrate $>50\,\%$), ISM predict a greater lipogenesis than IRM. ISM also predicts a greater diffusion coefficient while IRM displays a transient curve

Though the IRM rate of lipogenesis was found to be $1.2\,\mu m^2$/week for all diets 0–50 % carbohydrate, it may be that it exhibits a similar, albeit smaller decrease. The differences in v_{m0} predict that insulin resistant individuals will more easily gain weight while their insulin sensitive counterparts are slower to gain the same weight [3]. In contrast, differences in lipolysis and turnover between ISM and IRM during weight loss indicate that insulin resistant individuals will experience slower weight loss compared to their insulin sensitive counterparts (Fig. 11). The three insulin resistant groups exhibited narrow ranges for changes in D and v_{m0} during weight gain and weight loss, consistent with previous conclusions that insulin resistant adipocytes are less dynamic [36].

We used only the Gaussian component of the adipose cell size distribution but it may be that the parameters could be determined with greater precision by using the entire distribution. Note that the Gaussian approximation is best for the insulin sensitive groups. The adipose tissue dynamics model will need to include cell number changing processes for studies over longer time intervals [16]. Serial biopsies in subjects over the course of weight gain or loss would be a definitive test of the model comparison.

We have provided here a proof of principle that requiring the mathematical consistency of two physiological models of fat mass at different scales and incorporating different elements of subject data gives insight into changes in physiological processes in adipose tissue associated with insulin resistance.

7 Summary and Discussion

Adipose cell-size distributions represent traces of physical processes that individual adipose cells experience during their life. In the Chapter, we introduced how to infer dynamical processes from changes of static cell-size distributions using Bayesian inference. Given experimental data, mathematical modeling generally proposes possible hypothetical models that can explain the data. Bayesian inference plays a crucial role in obtaining the likelihood parameter values for given models, and quantitatively selecting the best model among them [21]. Therefore, this can serve as a general framework to infer underlying dynamics given data. For example, we have applied this to understand the development of pancreatic islets, the critical micro-organs for glucose metabolism [41].

Adipose cell-size distributions have long been measured in obesity research. However, mean cell size, obtained from the size distribution, was the single information practically used to examine hypertrophy and hyperplasia of adipose cells [4, 5]. Unlike these classic studies, the mathematical modeling of adipose cell-size distributions can provide substantially more information on adipose tissue dynamics. We could determine the cell-size dependency of adipose cell growth or shrinkage and death under positive/negative energy balance. In addition, cell-size fluctuations (lipid turnover) and cell turnover in adipose tissue are difficult to obtain experimentally. Therefore, mathematical modeling plays dual roles for integrating given data and for predicting physiological mechanisms that are not directly observable. The modeling is only as good as uncertainties in data allow. For example, the correct estimation of total cell number is critical because it affects the inference of cell recruitment and death. Although we deduced total cell number in adipose tissues from the tissue mass divided by the average mass of adipose cells, the number estimation could be erroneous due to an inaccurate measurement of the average cell mass. This uncertainty can ultimately be avoidable with direct measure of total cell number in adipose tissues. As another example, a fixed cell-size distribution can be explained alternatively as a stationary distribution exactly balancing cell recruitment, special growth, and death. Here direct measurements of one of these physical processes can easily check or rule out alternative possibilities. Therefore, for a better understanding of adipose tissue dynamics, theoretical modeling and experiment should complement each other.

This Chapter has focused on explaining the mechanistic building blocks of physical processes in modeling of adipose tissue dynamics. To complete the modeling, physiology of energy homeostasis needs to be incorporated into the present model so that each physical process is automatically controlled by

metabolism. For example, the amplitude and shape of the cell growth rate $v(s)$ should naturally vary depending on energy balance. Furthermore, the effect of insulin, regulating glucose metabolism, should also be incorporated into the growth rate $v(s)$. We took a first step towards this by comparing body composition predictions and adipose tissue predictions. A complete model may unify lipid and glucose metabolism, and provide a new platform for understanding metabolism. Such a model may also provide insight into how adipose tissue dynamics regulates energy storage capacity under the uncertainty of following food intakes and energy consumption.

References

1. Tchkonia, T., Corkey, B.E., Kirkland, J.L.: Current view of the fat cell as an endocrine cell: lipotoxicity. In: Bray, G.A., Ryand, D.H. (ed.) Overweight and the Metabolic Syndrome: From Bench to Bedside. Springer, Cambridge (2006)
2. Slawik, M., Vidal-Puig, J.: Lipotoxicity, overnutrition and energy metabolism in aging. Ageing Res. Rev. **5**, 144–164 (2006)
3. Spalding, K.L., Arner, E., Westermark, P.O., Bernard, S., Buchholz, B.A., Bergmann, O., Blomqvist, L., Hoffstedt, J., Näslund, E., Britton, T., Concha, H., Hassan, M., Rydén, M., Frisén, J., Arner, P.: Dynamics of fat cell turnover in humans. Nature **453**, 783–787 (2008)
4. Faust, I.M., Johnson, P.R., Hirsch, J.: Adipose tissue regeneration following lipectomy. Science **173**, 391–393 (1977)
5. Faust, I.M., Johnson, P.R., Stern, J.S., Hirsch, J.: Diet-induced adipocyte number increase in adult rats: a new model of obesity. Am. J. Physiol. **235**, E279–E286 (1977)
6. Pang, C., Gao, Z., Yin, J., Zhang, J., Jia, W., Ye, J.: Macrophage infiltration into adipose tissue may promote angiogenesis for adipose tissue remodeling in obesity. Am. J. Physiol. Endocrinol. Metab. **295**, E313–E322 (2008)
7. Lin, Y., Berg, A.H., Iyengar, P., Lam, T.K., Giacca, A., Combs, T.P., Rajala, M.W., Du, X., Rollman, B., Li, W., Hawkins, M., Barzilai, N., Rhodes, C.J., Fantus, I.G., Brownlee, M., Scherer, P.E.: The hyperglycemia-induced inflammatory response in adipocytes: the role of reactive oxygen species. J. Biol. Chem. **280**, 4617–4626 (2005)
8. Cinti, S., Mitchell, G., Barbatelli, G., Murano, I., Ceresi, E., Faloia, E., Wang, S., Fortier, M., Greenberg, A.S., Obin, M.S.: Adipocyte death defines macrophage localization and function in adipose tissue of obese mice and humans. J. Lipid Res. **46**, 2347–2355 (2005)
9. Monteiro, R., de Castro, P.M., Calhau, C., Azevedo, I.: Adipocyte size and liability to cell death. Obes. Surg. **16**, 804–806 (2006)
10. Björnheden, T., Jakubowicz, B., Levin, M., Odén, B., Edén, S., Sjöström, L., Lönn, M.: Computerized determination of adipocyte size. Obes. Res. **12**, 95–105 (2004)
11. Mersmann, H.J., MacNeil, M.D.: Variables in estimation of adipocyte size and number with a particle counter. J. Anim. Sci. **62**, 980–991 (1986)
12. McLaughlin, T., Sherman, A., Tsao, P., Gonzalez, O., Yee, G., Lamendola, C., Reaven, G.M., Cushman, S.W.: Enhanced proportion of small adipose cells in insulin-resistant vs insulin-sensitive obese individuals implicates impaired adipogenesis. Diabetologia **50**, 1707–1715 (2007)
13. Soula, H.A., Julienne, H., Soulage, C.O., Géloën, A.: Modelling adipocytes size distribution. J. Theor. Biol. **332**, 89–95 (2013)
14. Shoham, N., Gefen, A.: Stochastic modeling of adipogenesis in 3T3-L1 cultures to determine probabilities of events in the cell's life cycle. Ann. Biomed. Eng. **39**, 2637–53 (2011)

15. Vermolen, F.J., Segal, A., Gefen, A.: A pilot study of a phenomenological model of adipogenesis in maturing adipocytes using Cahn-Hilliard theory. Med. Biol. Eng. Comput. **49**, 1447–57 (2011)
16. Jo, J., Gavrilova, O., Pack, S., Jou, W., Mullen, S., Sumner, A.E., Cushman, S.W., Periwal, V.: Hypertrophy and/or hyperplasia: dynamics of adipose tissue growth. PLoS Comput. Biol. **5**, e1000324 (2009)
17. Jo, J., Guo, J., Liu, T., Mullen, S., Hall, K.D., Cushman, S.W., Periwal, V.: Hypertrophy-driven adipocyte death overwhelms recruitment under prolonged weight gain. Biophys. J. **99**, 3535–3544 (2010)
18. Jo, J., Kilimnik, G., Kim, A., Guo, C., Periwal, V., Hara, M.: Formation of pancreatic islets involves coordinated expansion of small islets and fission of large interconnected islet-like structures. Biophys. J. **101**, 565–574 (2011)
19. Sivia, D.S., Skilling, J.: Data Analysis: A Bayesian Tutorial, 2nd edn. Oxford University Press, New York (2006)
20. Jaynes, E.T.: Probability Theory: The Logic of Science. Cambridge University Press, New York (2003)
21. Gregory, P.C.: Bayesian Logical Data Analysis for the Physical Sciences. Cambridge University Press, Cambridge (2005)
22. Rodeheffer, M.S., Birsoy, K., Friedman, J.M.: Identification of white adipocyte progenitor cells in vivo. Cell **135**, 240–249 (2008)
23. Simon, G.: Histogenesis. In: Renold, A.E., Cahill, G.F. (eds.) Handbook of Physiology. Section 5: Adipose Tissue. American Physical Society, Washington DC (1965)
24. Jo, J., Shreif, Z., Periwal, V.: Quantitative dynamics of adipose cells. Adipocyte **1**, 80–88 (2012)
25. MacKellar, J., Cushman, S.W., Periwal, V.: Differential effects of thiazolidinediones on adipocyte growth and recruitment in Zucker fatty rats. PLoS One **4**, e8196 (2009)
26. Arner, P., Bernard, S., Salehpour, M., Possnert, G., Liebl, J., Steier, P., Buchholz, B.A., Eriksson, M., Arner, E., Hauner, H., Skurk, T., Rydén, M., Frayn, K.N., Spalding, K.L.: Dynamics of human adipose lipid turnover in health and metabolic disease. Nature **478**, 110–113 (2011)
27. Skurk, T., Alberti-Huber, C., Herder, C., Hauner, H.: Relationship between adipocyte size and adipokine expression and secretion. J. Clin. Endocrinol. Metab. **92**, 1023–1033 (2007)
28. Strissel, K.J., Stancheva, Z., Miyoshi, H., Perfield JW, 2.n.d., DeFuria, J., Jick, Z., Greenberg, A.S., Obin, M.S.: Adipocyte death, adipose tissue remodeling, and obesity complications. Diabetes **56**, 2910–2918 (2007)
29. Niesler, C.U., Siddle, K., Prins, J.B.: Human preadipocytes display a depot-specific susceptibility to apoptosis. Diabetes **47**, 1365–1368 (1998)
30. MacKellar, J., Cushman, S.W., Periwal, V.: Waves of adipose tissue growth in the genetically obese Zucker fatty rat. PLoS One **5**, e8197 (2010)
31. Kirkpatrick, S., Gelatt, C.D., Vecchi, M.P.: Optimization by simulated annealing. Science **220**, 671–680 (1983)
32. Corana, A., Marchesi, M., Martini, C., Ridella, S.: Minimizing multimodal functions of continuous variables with the "simulated annealing" algorithm. ACM Trans. Math. Softw. **13**, 262–280 (1987)
33. Hall, K.D., Sacks, G., Chandramohan, D., Chow, C.C., Wang, Y.C. et al.: Quantification of the effect of energy imbalance on bodyweight. Lancet **378**(9793), 826837 (2011)
34. Johannsen, D.L., Knuth, N.D., Huizenga, R., Rood, J.C., Ravussin, E. et al.: Metabolic slowing with massive weight loss despite preservation of fat-free mass. J. Clin. Endocrinol. Metab. **97**(7), 248996 (2012)
35. Kursawe, R., Eszlinger, M., Narayan, D., Liu, T., Bazuine, M. et al.: Cellularity and adipogenic profile of the abdominal subcutaneous adipose tissue from obese adolescents: association with insulin resistance and hepatic steatosis. Diabetes **59**(9), 228896 (2010)

36. Yang, J., Eliasson, B., Smith, U., Cushman, S.W., Sherman, A.S.: The size of large adipose cells is a predictor of insulin resistance in first-degree relatives of type 2 diabetic patients. Obesity **20**(5), 9328 (2012)
37. Frayn, K., Bernard, S., Spalding, K., Arner, P.: Adipocyte triglyceride turnover is independently associated with atherogenic dyslipidemia. J. Am. Heart Assoc. **1**(6), e003467 (2012)
38. Laurencikiene, J., Skurk, T., Kulyt, A., Hedn, P., Astrm, G. et al.: Regulation of lipolysis in small and large fat cells of the same subject. J. Clin. Endocrinol. Metab. **96**(12), E20459 (2011)
39. Koutsari, C., Basu, R., Rizza, R.A., Nair, K.S., Khosla, S. et al.: Nonoxidative free fatty acid disposal is greater in young women than men. J. Clin. Endocrinol. Metab. **96**(2), 541547 (2011)
40. Horton, T.J., Dow, S., Armstrong, M., Donahoo, W.T.: Greater systemic lipolysis in women compared with men during moderate-dose infusion of epinephrine and/or norepinephrine. J. Appl. Physiol. **107**(1), 200210 (2009)
41. Jo, J., Hara, M., Ahlgren, U., Sorenson, R., Periwal, V.: Mathematical models of pancreatic islet size distributions. Islets **4**, 10–19 (2012)

http://www.springer.com/978-3-319-09335-2

The Mechanobiology of Obesity and Related Diseases
Gefen, A.; Benayahu, D. (Eds.)
2015, X, 296 p., Hardcover
ISBN: 978-3-319-09335-2